ELSEVIER

Journal of Nuclear Materials 244 (1997) 258–265

journal of nuclear materials

Temperature and dose dependence of ion-beam-induced amorphization in α-SiC

W.J. Weber [a,*], N. Yu [b,1], L.M. Wang [c], N.J. Hess [a]

[a] *Pacific Northwest National Laboratory, P.O. Box 999, Richland, WA 99352, USA*
[b] *Materials Science and Technology Division, Los Alamos National Laboratory, Los Alamos, NM 87545, USA*
[c] *Department of Earth and Planetary Sciences, University of New Mexico, Albuquerque, NM 87131, USA*

Received 5 February 1996; accepted 23 August 1996

Abstract

Single crystal α-SiC with [0001] orientation has been irradiated at 170, 300, and 370 K with 360 keV Ar^{2+} ions at an incident angle of 25° and the damage accumulation process followed in situ by Rutherford backscattering spectroscopy in channeling geometry (RBS/C) along [$1\bar{1}02$]. At 170 and 300 K, the increase in relative disorder with ion fluence, as measured by RBS/C, is consistent with a multiple-cascade overlap process. There is a significant deviation from the cascade overlap model at 370 K. The RBS/C results indicate that below a critical damage level the relative disordering rate is nearly temperature independent. Post-irradiation characterization of the fully disordered samples indicate a significant loss in the intensity of the Raman modes and decreases of 47 and 24% in hardness and elastic modulus, respectively. Cross sectional transmission electron microscopy has confirmed the amorphous nature of the damaged surface layer irradiated at 170 K; however, at 370 K, some residual crystallinity was observed over the depth range from 10 to 160 nm. The decrease in density associated with amorphization at 170 K is estimated to be $22 \pm 3\%$.

1. Introduction

Silicon carbide (SiC) is an important technological material with high-temperature semiconducting properties, high thermal conductivity, high-temperature stability, extreme hardness, and chemical inertness. It is a promising wide-gap semiconductor for high-temperature, high-power, and high-speed electronic devices. Because of its small neutron capture cross-section, SiC also is a candidate material for structural components in fusion reactor systems and is proposed as an inert host matrix for the burnup of excess weapons plutonium using nuclear reactors or accelerator-based neutron sources. Electronic device fabrication, long-term performance in a fusion-reactor or other high-radiation environments, and ion-beam modification/processing of high-temperature structural components require detailed understanding of irradiation effects in SiC, in particular the kinetics of defect accumulation and amorphization processes.

There are well over 100 polymorphs of SiC that exist; however, α-SiC (6H polytype) and β-SiC (3C polytype) are of the most technological interest [1]. Ion-beam-induced amorphization in α-SiC at room temperature [1–9] and in β-SiC [9,10] at room and liquid nitrogen temperatures has been studied in detail. Recently, the temperature dependence of ion-beam-induced amorphization in α-SiC [11–14] and β-SiC [15] has been investigated. Complete amorphization in SiC occurs for damage energies of about 14 to 17 eV/atom below liquid nitrogen temperature and 20 to 25 eV/atom at room temperature. Electron-beam-induced amorphization in α-SiC [16–18] and β-SiC [19] over a wide range of temperatures also has been investigated. The critical damage energies at low temperatures for complete amorphization under 2 MeV electron irradiation are up to a factor of four higher than under 1.5 MeV Xe^+ irradiation for α-SiC [13] and β-SiC [15]. In addition, the

* Corresponding author. E-mail: wj_weber@pnl.gov.
[1] Current address: Semiconductor Process and Device Center, Texas Instruments, Inc., Dallas, TX 75243, USA.

PII S0022-3115(96)00742-8

critical damage energies in α-SiC under electron irradiation exhibit a significant dependence on crystallographic orientation [16]. Chemical disordering also has been reported to play an important role in the crystalline-to-amorphous transition in α-SiC [18] and β-SiC [19] under electron irradiation. In α-SiC, the critical damage energy for complete amorphization increases with temperature in two stages and rises rapidly at temperatures above 200 K [13,16]. The critical temperatures, T_c, above which amorphization cannot be induced in α-SiC are estimated to be 290 K for 2 MeV electrons [16], 420 K for 0.56 MeV Si^+ [14], 485 K for 1.5 MeV Xe^+ [13], and 573 K for 0.23 MeV Ga^+. In β-SiC, the critical temperatures are slightly higher and estimated to be 340 K for 2 MeV electrons [9] and 498 K for 1.5 MeV Xe^+ [15].

In general, the dose dependence of damage accumulation and amorphization at different temperatures has been studied using ex situ characterization techniques at room temperature, such as Rutherford backscattering spectroscopy in channeling geometry (RBS/C) [10–12] and cross-sectional transmission electron microscopy (XTEM) [9,12,14]. For irradiations at low temperatures, damage annealing may occur prior to or during transfer, preparation, and characterization at room temperature. Recently, the authors have used the HVEM/Tandem Irradiation Facility at Argonne National Laboratory [20] to study in situ the temperature dependence of the critical dose (damage energy) for amorphization in α-SiC [13] and β-SiC [15]; however, quantitative details of the damage accumulation as a function of cumulative dose are not easily determined by these experiments. In the present paper, the results of a recent investigation that utilizes in situ RBS/C, during 360 keV Ar^{2+} irradiation, to measure the dose dependence of damage accumulation and amorphization in α-SiC at different temperatures are reported.

2. Experimental procedures

The n-type α-SiC (6H polytype) single crystal wafer used in this study was obtained from Cree Research and was oriented on the [0001] axis. Irradiations at 170, 300, and 370 K with 360 keV Ar^{2+} ions at a flux of 4×10^{12} ions/cm^{2}s were carried out on an as-received polished (Si face) wafer using the dual-beam facilities within the Ion Beam Materials Laboratory at Los Alamos National Laboratory [21]. The two beamlines for the ion irradiations and the RBS/C analysis are at a relative angle of 60°, which required that both the ion irradiations and the RBS/C measurements be carried out at fairly large angles off the surface normal. The single crystal wafer was oriented such that it was irradiated with 360 keV Ar^{2+} ions at $\sim 25°$ off the [0001] axis over an area of 10 mm diameter. An in situ RBS/C analysis was obtained at temperature on the virgin specimen area and after each incremental ion fluence, using a 2 MeV He^+ ion beam (2 mm spot size) incident along the [1$\bar{1}$02] channeling direction ($\sim 35.2°$ off the [0001] axis), in the center of the irradiated area, and a backscattering angle of 165°. This orientation provided the optimum channeling direction given the constraints of the experimental geometry. For channeling along this direction, the measured value of χ_{min}, which is defined as the ratio of the backscattering yield in the virgin spectrum just below the surface peak to the yield in the random spectrum, was 0.05 in the SiC. The irradiations at each temperature were continued until the RBS/C spectrum indicated that the entire irradiated layer, from the surface to the end of range, was fully disordered (i.e., the aligned backscattering yield reached the fully random level). The crystal wafer was translated vertically (perpendicular to the beam direction) to provide a different area for irradiation at each temperature.

Post-irradiation characterization of the fully-disordered samples produced at each irradiation temperature was carried out at room temperature and included Raman spectroscopy, mechanical property microprobe, and cross-sectional transmission electron microscopy (XTEM). Since epitaxial recrystallization of amorphous layers in SiC requires temperatures above 1700 K [1], recovery of the fully-disordered samples was not expected at room temperature. The Raman spectroscopy was performed with 488.0 nm radiation at the Pacific Northwest National Laboratory. The mechanical microprobe (nano-indentation) measurements of hardness and elastic modulus were performed by Nano Instruments, of Oak Ridge, TN. Ten indents at nominal displacements of 20, 40, and 80 nm were made on unirradiated and irradiated samples. The XTEM was performed within the High-Resolution Analytical Electron Microscopy Laboratory at the University of New Mexico using a JEOL 2010 microscope operated at 200 kV. The XTEM specimens were prepared by cutting each sample in half, gluing the two irradiated surfaces together, sectioning the crystals perpendicular to the irradiated surface, and cutting 3 mm discs from the cross sections; the disks were then mechanically thinned and ion milled.

The density of atomic displacements produced per ion as a function of depth under the irradiation conditions for both the 360 keV Ar^{2+} and 2 MeV He^+ was determined from full cascade Monte Carlo calculations using TRIM-96 [22], which is part of the renamed SRIM-96 (Stopping and Range of Ions in Matter) program. In these calculations, a displacement energy of 25 eV for both Si and C was used. (The displacement energy for C in α-SiC is reported to be ~ 22 eV [23], and the displacement energy for Si is assumed by the authors to be similar.) The calculated distribution of displaced atoms in α-SiC under the irradiation conditions employed are shown in Fig. 1 for a typical incremental fluence of 360 keV Ar^{2+} ions and for a 2 MeV He^+ (RBS/C) analysis. Each RBS/C analysis was performed to an integrated fluence of 40 He^+ ions/nm^2, which contributed 1.5×10^{-3} dpa to the incremental dose from the 360 keV Ar^{2+} ions. Since the 2 MeV He^+ probe

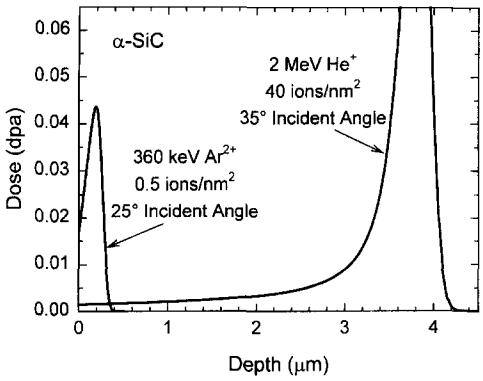

Fig. 1. Damage distributions in α-SiC irradiated to incremental fluences with 360 keV Ar^{2+} ions at 25° incident angle and with 2 MeV He^{+} ions at 35° incident angle (calculated using TRIM-96).

contributes slightly to the overall cumulative damage produced by the 360 keV Ar^{2+} ions during the in situ experiments, the total dose, in units of displacements per atom (dpa), reported below includes the contribution from the RBS/C He^{+} beam. (Note: previous studies of SiC by the authors [13,15] used TRIM-95, which underestimated the displacements produced as a result of an error in the calculation of electronic stopping powers for SiC.)

3. Results and discussion

3.1. In situ RBS/C analysis

For each sample area irradiated, the 2 MeV He^{+} beam for the RBS/C analysis was aligned with the bulk [1$\bar{1}$02] direction, and a RBS/C spectrum of the virgin (unirradiated) area was taken at the preset temperature prior to initiating the irradiation sequence. The irradiation sequence involved irradiating the selected area with an incremental fluence of 360 keV Ar^{2+} ions followed by an RBS/C analysis, with its incremental fluence. The irradiation sequences at 170 and 300 K involved 17 irradiation steps and RBS/C spectra. At 370 K, 18 irradiation steps and spectra were taken. Several of the sequential RBS/C spectra taken as a function of ion fluence during irradiations at 170, 300, and 370 K are shown in Figs. 2–4, respectively. Also shown is the spectrum from the unirradiated virgin sample and a random spectrum obtained by

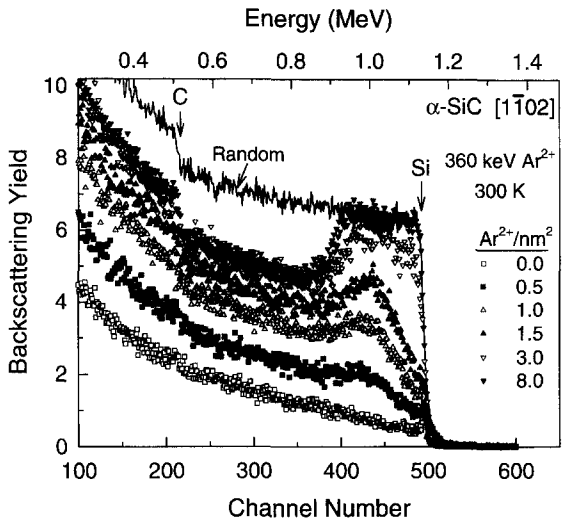

Fig. 3. Several of the aligned backscattering spectra obtained in situ from α-SiC irradiated sequentially with 360 keV Ar^{2+} ions at 300 K, along with a random spectrum.

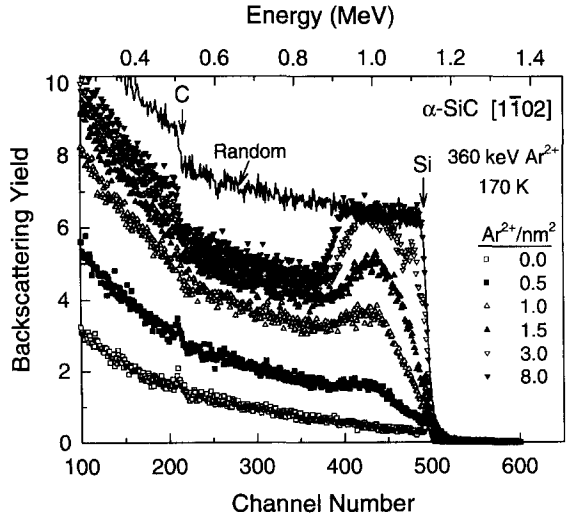

Fig. 2. Several of the aligned backscattering spectra obtained in situ from α-SiC irradiated sequentially with 360 keV Ar^{2+} ions at 170 K, along with a random spectrum.

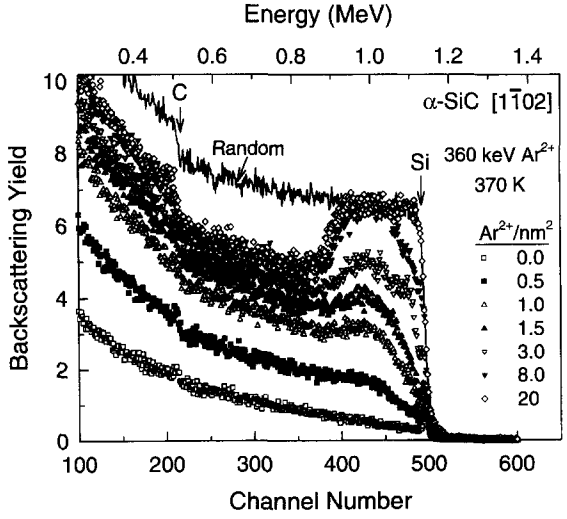

Fig. 4. Several of the aligned backscattering spectra obtained in situ from α-SiC irradiated sequentially with 360 keV Ar^{2+} ions at 370 K, along with a random spectrum.

rocking the incident angle a few degrees off the channeling direction. The increase in the backscattering (dechanneling) yield from the Si atoms provides a profile of the distribution of displaced Si atoms on the Si sublattice. At 170 K, the dechanneling yield from the Si reaches the random level at a fluence of 4.0 Ar^{2+} ions/nm^2. The fluence at which the dechanneling yield from Si first reaches the random level increases with temperature to 5.0 Ar^{2+} ions/nm^2 and 10.0 Ar^{2+} ions/nm^2 for the irradiations at 300 and 370 K, respectively. Much higher fluences (nearly a factor of two) are required for the surface regions to be randomized. At the higher fluences for each temperature, the dechanneling yield from the C atoms also noticeably increases and at the highest fluences is consistent with a random yield. (There is no discernable loss of C in the near-surface spectra.) At fluences above 2.5 ions/nm^2 (3.0 ions/nm^2 in Figs. 2–4), where the main peak in the backscattering yield is near or at the random level, another smaller peak in the backscattering yield is observed just below the surface. This peak is similar to that reported by Edmond et al. in β-SiC [10] and by Holland et al. in Si [24] and is evidence for misalignment of the residual crystalline material in front of the buried amorphous layer with respect to the aligned crystalline substrate beyond the amorphous layer. This misalignment is the result of the large change in density (15 to 17% volume expansion at room temperature [1,9]) associated with amorphization in SiC. As the damage accumulates, it is expected that the density in the irradiated layer changes nonuniformly with depth and nonlinearly with fluence.

Since the energy of the backscattered He^+ ions is linearly related to the areal density of atoms (atoms/nm^2) in the traversed layer [25], profiles of the dechanneling yield from the Si atoms have been obtained from the RBS/C spectra as a function of the areal atomic density, which can be equated to depth only if the density is constant or if the density distribution is known. Using the procedure described by Holland et al. [26], the relative disorder along the [1$\bar{1}$02] direction has been determined from the profiles of the backscattering yields of aligned and random spectra. The relative disorder at 170 K as a function of traversed atomic density for several ion fluences is shown in Fig. 5, also included is a depth scale referenced to the density of the undamaged SiC. The relative disorder in the irradiated layer increases with ion fluence at all temperatures and becomes coincident with the fully disordered (random) level at a traversed atomic density corresponding to the peak in the ion-damage profile. As the ion fluence increases further, the width of the fully disordered layer increases and eventually consumes the entire irradiated layer. As discussed by Edmond et al. for β-SiC [10], the random level for dechanneling along a given direction may not always correspond to a fully amorphous state, and this may be the case for dechanneling along the [1$\bar{1}$02] direction in this study, as discussed below for the XTEM results. The distribution of the relative disorder in the irradiated layer at 170 K for a fluence of 3.0 Ar^{2+} ions/nm^2 is shown in Fig. 6 and is in excellent agreement with the ion-damage profile, also shown, that is predicted by TRIM-96 calculations. The anomalous peak in the relative disorder (misalignment of the near surface crystalline material) that is observed in the profiles (e.g., Figs. 5 and 6) for fluences greater than 2.5 ions/nm^2 occurs over a depth range corresponding to 20 to 60 nm in the undamaged SiC. This near-surface peak was not included in the curve fitting analyses.

The ingrowth of the relative disorder at the surface and at the peak in the damage profile were determined for each

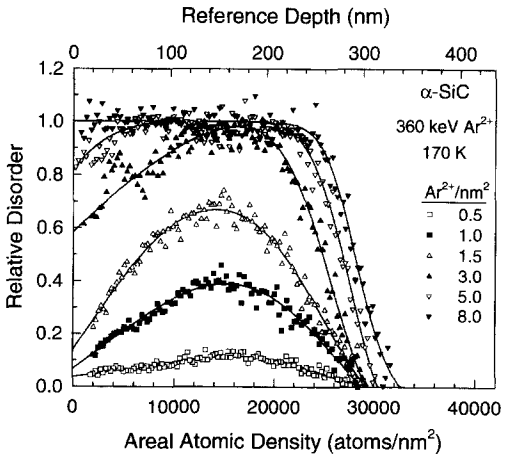

Fig. 5. Profiles of the relative disorder as a function of traversed atom density in α-SiC irradiated at 170 K (also included is a depth scale referenced to the density of the undamaged SiC). The results are derived from the RBS/C spectra in Fig. 2.

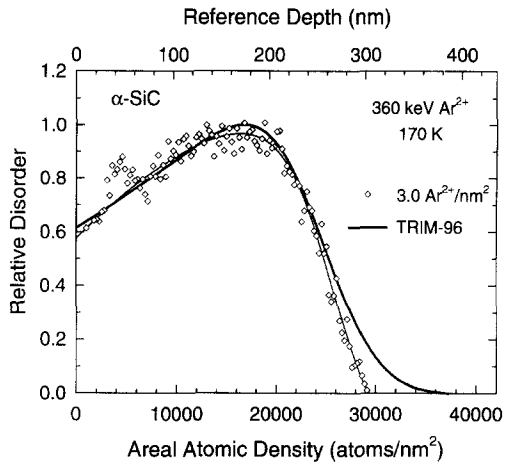

Fig. 6. Comparison of the relative disorder profile in α-SiC irradiated to 3.0 Ar^{2+} ions/nm^2 at 170 K and the normalized damage distribution calculated by TRIM-96.

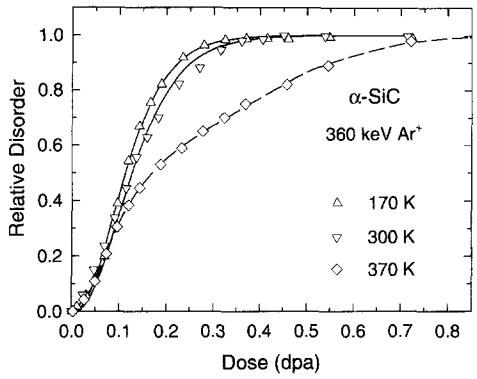

Fig. 7. Relative disorder, determined at the peak in the damage profile, as a function of dose (dpa) for α-SiC irradiated at 170, 300, and 370 K. (Solid curves are fits of the double-overlap model (Eq. (1)), and the dashed curve is a polynomial fit.)

spectrum. When compared on a basis of the calculated displaced atom dose (dpa), the relative disorder at the surface and at the damage peak exhibited a similar dependence on dose at each temperature, suggesting a minimal effect of the surface on the disordering process. The relative disorder at the peak in the damage profile is shown in Fig. 7 as a function of the displacement dose and irradiation temperature. The rate of disordering decreases with increasing temperature, consistent with an increase in defect recovery processes at elevated temperatures; however, the results suggest that there is a critical level of damage (defect concentration), corresponding to a relative disorder value of about 0.3, below which the disorder is largely temperature independent. The relative disorder at 170 and 300 K follows a nearly sigmoidal dependence on dose that is consistent with the double-cascade overlap model for amorphization defined by Gibbons [27], which is shown by the curve fits at these two temperatures. In this model, the amorphous fraction, f_a, is given by

$$f_a = 1 - \left[\left(1 + BD + B^2D^2/2\right)\exp(-BD)\right] \quad (1)$$

where B is related to the effective damage volume per ion and D is the dose. The value of B determined by nonlinear regression analysis decreases from 24 dpa^{-1} at 170 K to 21 dpa^{-1} at 300 K, indicating a decrease in the effective damage volume with increasing temperature. At 370 K, the dose dependence of the relative disorder markedly deviates from the double-overlap model after the disorder reaches a value of about 0.4; this behavior may be due to significant defect interactions, recovery, and/or migration at this temperature.

3.2. Temperature dependence of critical dose

From the RBS/C results in Fig. 7, the critical dose for amorphization can be estimated as the dose when the relative disorder reaches unity at each irradiation temperature. The results are shown in Fig. 8, along with the results of Weber et al. [13] for 1.5 MeV Xe^+ irradiations along [0001] (dose corrected using TRIM-96) and the results of Inui et al. [16] for 2 MeV electron irradiations along [0001], [11$\bar{2}$0], and [1$\bar{1}$00]. The model and activation energy derived previously [13] for the 1.5 MeV Xe^+ and 2 MeV electron data are used to fit the curve (shown) to the 360 keV Ar^{2+} data. Below 300 K, the critical amorphization dose for the 360 keV Ar^{2+} irradiations at 25° off the [0001] direction is lower than the corresponding critical dose for 1.5 MeV Xe^+ irradiation along the [0001] direction. This may be associated with an effect of crystallographic orientation during irradiation, as suggested by the 2 MeV electron results [16] that indicate irradiations along the [0001] direction have a higher critical dose; it also may be due to the effect of channeling direction on determining amorphization, as discussed by Edmond et al. [10]. The results in Fig. 8 also show that above 300 K the amorphization dose for 360 keV Ar^{2+} rises more rapidly with temperature than for the 1.5 MeV Xe^+ irradiations, which suggests a lower critical temperature for the 360 keV Ar^{2+} irradiations than for the 1.5 MeV Xe^+ (yet higher than for the 2 MeV electrons). The critical temperature for amorphization in α-SiC under 360 keV Ar^{2+} irradiation is estimated to be 425 K from the curve fit. The decrease in critical temperature with decreasing projectile mass is similar to the behavior that has been reported previously for SiC [13,15], Si [28], $Ca_2La_8(SiO_4)_6O_2$ [29], and CuTi [30]. This behavior is attributed to a decrease in the size of the recoil cascades and an increase in freely migrating defects with decreasing mass of the incident ion.

3.3. Optical and mechanical properties

Raman spectroscopy with 488.0 nm radiation was carried out on an unirradiated sample and on the fully-disordered samples produced at each irradiation temperature.

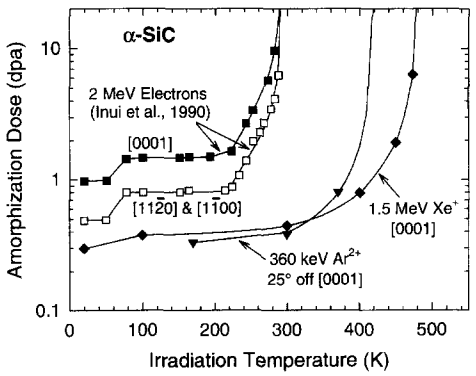

Fig. 8. Temperature dependence of the dose to amorphize α-SiC for 360 keV Ar^{2+} (this study), for 1.5 MeV Xe^+ [13] (dose corrected using TRIM-96), and for 2 MeV electrons at different orientations [16].

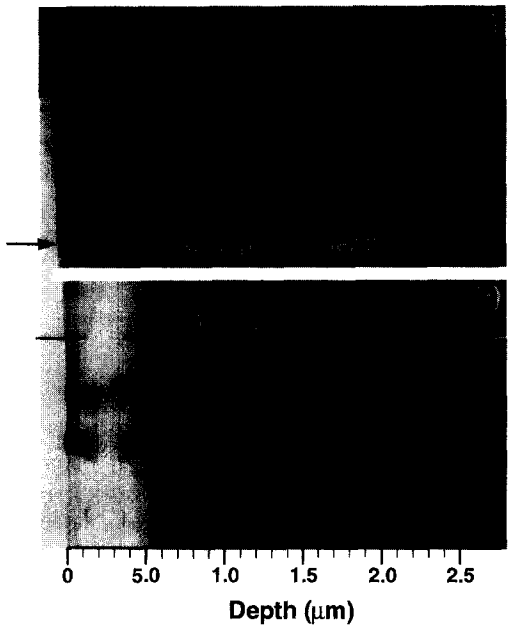

Fig. 9. XTEM images of samples irradiated with 360 keV Ar^{2+} to (a) 8 ions/nm^2 at 170 K and (b) 20 ions/nm^2 at 370 K.

The intensity of the first-order Raman vibrational modes in α-SiC that were observed in the unirradiated material were completely absent in all the irradiated materials, which is consistent with an amorphous or highly disordered state. Similar results have been reported by McHargue et al. [31]. The results of the nano-indentation measurements show a significant decrease in the hardness and elastic modulus of the disordered (amorphous) layer of the sample irradiated at 170 K to 8.0 Ar^{2+} ions/nm^2 (the other two samples were not measured). The hardness decreased 47% (from 49 to 26 GPa), and the elastic modulus decreased 24% (from 550 to 418 GPa). These results are similar to those reported by McHargue and Williams [1]. Further details on the dose dependence of the changes in Raman intensity and mechanical properties will be determined as part of an ongoing investigation of α-SiC.

3.4. XTEM analysis

Post-irradiation XTEM was performed on the specimens studied in situ with RBS/C; consequently, the images correspond to the maximum dose where the RBS/C results suggest full disorder from the surface to the end of range. XTEM micrographs of samples irradiated at 170 and 370 K are shown in Fig. 9. (XTEM specimen preparation from the sample irradiated at 300 K was not successful.) In the specimen irradiated at 170 K to 8 ions/nm^2 (Fig. 9(a)), a completely amorphous layer was observed that extends from the surface to a depth of 365 nm. This result is consistent with the RBS/C result that shows a fully-disordered layer that is coincident with the areal atomic density of the irradiated layer predicted by TRIM. Using the traversed atom density of the fully-disordered layer determined by RBS/C and the layer thickness determined by XTEM, the density of the amorphous state at 170 K is estimated to be 2.47 ± 0.10 g/cm^3. This decrease in density of $23 \pm 3\%$ at this temperature is larger than the 15 to 17% volume expansion [1,9] reported for SiC at room temperature. In the XTEM specimen prepared from the sample irradiated at 370 K to 20 ions/nm^2, two amorphous bands were observed, as shown by the micrograph in Fig. 9(b). The deeper band is believed to be the result of damage from the 2 MeV He^+ probe that corresponds to a fluence of 400 ions/nm^2 in this XTEM specimen, which was inadvertently cut from an irradiated region that included the region probed by the He^+ beam during RBS/C analysis. This deeper amorphous band is about 400 nm thick and starts at a depth of 2.1 μm, which is considerably less than the projected peak in the damage profile (3.8 μm), calculated by TRIM-96, for 2 MeV He^+ under these irradiation conditions. The shallower amorphous band that extends from 160 to 360 nm is a result of damage from the 360 keV Ar^{2+} irradiation. In addition to the two observable amorphous bands in Fig. 9(b), there also is an 8 nm thick amorphous layer at the surface (discussed below). Residual crystallinity is clearly evident over the depth from 8 to 160 nm at this orientation (Fig. 9(b)), even though the RBS/C spectra along the [1$\bar{1}$02] direction from this layer indicates complete disorder. This is consistent with the observations of Edmond et al. [10] on β-SiC regarding the effect of orientation on determining complete amorphization by RBS/C. Although the irradiated layer at 370 K is not amorphous over its whole thickness, it is significantly damaged, and the average decrease in density associated with the observed damage, based on the RBS/C and XTEM results, is $16 \pm 3\%$.

In the XTEM specimen irradiated at 170 K, high-resolution TEM (HRTEM) was carried out in a thin region at the end of the Ar ion range. The HRTEM micrograph from

Fig. 10. HRTEM image of the amorphous/crystalline interface at the end of range (365 nm) in a cross section of the sample irradiated with 360 keV Ar^{2+} to 8 ions/nm^2 at 170 K.

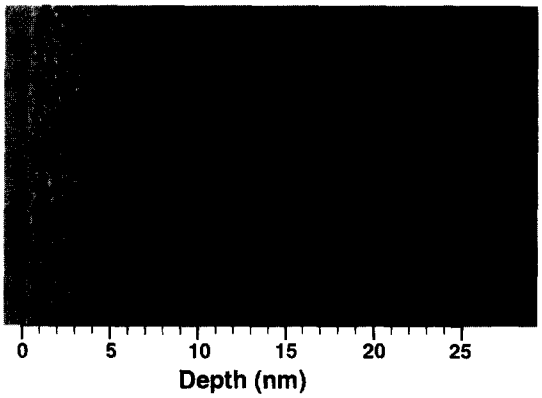

Fig. 11. HRTEM image of the surface region in a cross section of the sample irradiated with 360 keV Ar^{2+} to 20 ions/nm^2 at 370 K.

the end of range (Fig. 10) shows the transitional interface (~ 20 nm) between the irradiation-induced amorphous layer and the crystalline substrate, including a few residual crystalline islands in the amorphous matrix. A HRTEM image of the surface of the specimen irradiated at 370 K is shown in Fig. 11. The amorphous layer at the surface extends from the surface to a depth of about 8 nm. Beyond that depth, the image shows evidence for some weak unconnected periodicity in the matrix, which indicates that the matrix in this region is not yet completely transformed to the amorphous state.

4. Summary

In situ RBS/C techniques have been used to study the accumulation of ion-beam-induced disorder in α-SiC along the $[1\bar{1}02]$ direction. The relative disorder measured by RBS/C increases with dose at 170 and 300 K and follows a dependence that is consistent with the double-cascade overlap model for amorphization. At 370 K, there is a significant deviation from the predicted model behavior due to defect recovery and/or migration. The RBS/C results indicate that below a critical damage level the relative disorder is largely temperature independent. The critical temperature for amorphization under 360 keV Ar^{2+} irradiation is estimated to be 425 K. Post-irradiation characterization of the fully disordered samples indicate a significant loss in the intensity of the Raman modes and decreases in hardness and elastic modulus of 48 and 24%, respectively. The decrease in density associated with amorphization at 170 K is estimated to be $22 \pm 3\%$.

Acknowledgements

The authors thank M. Nastasi, J.R. Tesmer, and the staff of the Ion Beam Materials Laboratory at Los Alamos National Laboratory for their assistance with the ion irradiations and Y. Guo of the University of New Mexico for the XTEM sample preparation. This research was supported by the Division of Materials Sciences, Office of Basic Energy Sciences, U.S. Department of Energy under Contract DE-AC06-76RLO 1830 (PNNL) and Contract W-7405-ENG-36 (LANL).

References

[1] C.J. McHargue and J.M. Williams, Nucl. Instrum. Methods B 80–81 (1993) 889.
[2] R.R. Hart, H.L. Dunlap and O.J. Marsh, Radiat. Eff. 9 (1971) 261.
[3] J.A. Spitznagel, S. Wood, W.J. Choyke, N.J. Doyle, J. Bradshaw and S.G. Rishman, Nucl. Instrum. Methods B 16 (1986) 23.
[4] T. Hioki, A. Itho, M. Ohkubo, S. Noda, H. Doi, J. Kawamoto and O. Kamigaito, J. Mater. Sci. 21 (1986) 1321.
[5] C.J. McHargue, D.L. Joslin and J.M. Williams, Nucl. Instrum. Methods B 46 (1990) 185.
[6] A. Föhl, R.M. Emrick and H.D. Carstanjen, Nucl. Instrum. Methods B 65 (1992) 335.
[7] N.G. Chechenin, K.K. Bourdelle, A.V. Suvorov and A.X. Kastilio-Vitloch, Nucl. Instrum. Methods B 65 (1992) 341.
[8] L.L. Horton, J. Bentley, L. Romana, A. Perez, C.J. Mchargue and J.C. McCallum, Nucl. Instrum. Methods B 65 (1992) 345.
[9] L.L. Snead and S.J. Zinkle, in: Microstructure of Irradiated Materials, eds. I.M. Robertson, L.E. Rehn, S.J. Zinkle and W.J. Phythian (Materials Research Society, Symp. Proc. 373, Pittsburgh, PA, 1995) p. 377.
[10] J.A. Edmond, R.F. Davis, S.P. Withrow and K.L. More, J. Mater. Res. 3 (1988) 321.
[11] A. Heft, E. Wendler, T. Bachmann, E. Glaser and W. Wesch, Mater. Sci. Eng. B 29 (1995) 142.
[12] W. Wesch, A. Heft, E. Wendler, T. Bachmann and E. Glaser, Nucl. Instrum. Methods B 96 (1995) 335.
[13] W.J. Weber, L.M. Wang and N. Yu, Nucl. Instrum. Methods B116 (1996) 322.
[14] S.J. Zinkle and L.L. Snead, Nucl. Instrum. Methods B116 (1996) 92.
[15] W.J. Weber and L.M. Wang, Nucl. Instrum. Methods B 106 (1995) 298.
[16] H. Inui, H. Mori and H. Fujita, Philos. Mag. B 61 (1990) 107.
[17] A. Matsunaga, C. Kinoshita, K. Nakai and Y. Tomokiyo, J. Nucl. Mater. 179–181 (1991) 457.
[18] H. Inui, H. Mori and T. Sakata, Philos. Mag. B 66 (1992) 737.
[19] H. Inui, H. Mori, A. Suzuki and H. Fujita, Philos. Mag. B 65 (1992) 1.
[20] C.W. Allen, L.L. Funk, E.A. Ryan and A. Taylor, Nucl. Instrum. Methods B 40–41 (1989) 553.
[21] N. Yu, M. Nastasi, T.E. Levine, J.R. Tesmer, M.G. Hollander, C.R. Evans and C.J. Maggiore, Nucl. Instrum. Methods B99 (1995) 566; N. Yu, T.E. Levine, K.E. Sickafus, M. Nastasi, J.N. Mitchell, C.J. Maggiore, C.R. Evans, M.G.

Hollander, J.R. Tesmer, W.J. Weber and J.W. Mayer, Nucl. Instrum. Methods B118 (1996) 766.
[22] J.F. Ziegler, J.P. Biersack and U. Littmark, The Stopping and Range of Ions in Solids (Pergamon Press, New York, 1985).
[23] A.L. Barry, B. Lehmann, D. Fritsch and D. Bräunig, IEEE Trans. Nucl. Sci. 38 (1991) 1111.
[24] O.W. Holland, J.D. Budai and C.W. White, Appl. Phys. Lett. 57 (1990) 243.
[25] L.C. Feldman and J.W. Mayer, Fundamentals of Surface and Thin Film Analysis (North Holland, New York, 1986) p. 48.
[26] O.W. Holland, D. Fathy, J. Narayan and O.S. Oen, Radiat. Eff. 90 (1985) 127.
[27] J.F. Gibbons, Proc. IEEE 60 (1972) 1062.
[28] F.F. Morehead and B.L. Crowder, Radiat. Eff. 6 (1970) 27.
[29] W.J. Weber and L.M. Wang, Nucl. Instrum. Methods B 91 (1994) 63.
[30] J. Koike, P.R. Okamoto and L.E. Rehn, J. Mater. Res. 4(5) (1989) 1143.
[31] C.J. McHargue, P.S. Sklad and C.W. White, Nucl. Instrum. Methods B 46 (1990) 79.